Photochemical & Photobiological Sciences
https://doi.org/10.1007/s43630-025-00684-0

ORIGINAL PAPERS

Solvatochromism and *cis–trans* isomerism in azobenzene-4-sulfonyl chloride

İsa Sıdır[1] · Yadigar Gülseven Sıdır[1] · Halil Berber[2] · Rui Fausto[3,4]

Received: 15 October 2024 / Accepted: 10 January 2025

Abstract

Solvatochromism exhibited by azobenzene-4-sulfonyl chloride (here abbreviated as Azo-SCl) has been investigated in a series of non-polar, polar-aprotic and polar-protic solvents. The UV–vis spectra of Azo-SCl exhibit two long-wavelength bands, observed at 321–330 nm (band-I) and 435–461 nm (band-II), which are ascribed to the π*-π ($S_2 \leftarrow S_0$) and π*-n ($S_1 \leftarrow S_0$) transitions, respectively. The shorter wavelength band indicates a reversal in solvatochromism, from negative to positive solvatochromism, for a solvent with a dielectric constant of 32.66 (which is characteristic of methanol), while the longer wavelength band signposts negative solvatochromism in all range of solvent's dielectric constant investigated, demonstrating different interactions with the solvents in the S_2 and S_1 excited states. Using Catalán and Kamlet-Taft solvation energy models, we found that the shift in the solvatochromic behavior of band-I ($S_2 \leftarrow S_0$) happens because solvent dipolarity/polarizability and hydrogen bonding affect the S_2 state in opposite ways. Dipolarity/polarizability stabilizes the S_2 state compared to the ground state, while hydrogen bonding destabilizes it. In contrast, for S_1, both effects work together to destabilize the excited state. For all studied solvents, UV irradiation ($\lambda \geq 311$ nm; room temperature) was found to lead to fast *trans–cis* azo photoisomerization. In the absence of light, the photogenerated *cis* form quickly converts back to the *trans* form. Interpretation of the experimental data is supported by quantum chemical calculations undertaken within the Density Functional Theory (DFT) framework, including Time Dependent DFT calculations for excited states.

Graphical abstract

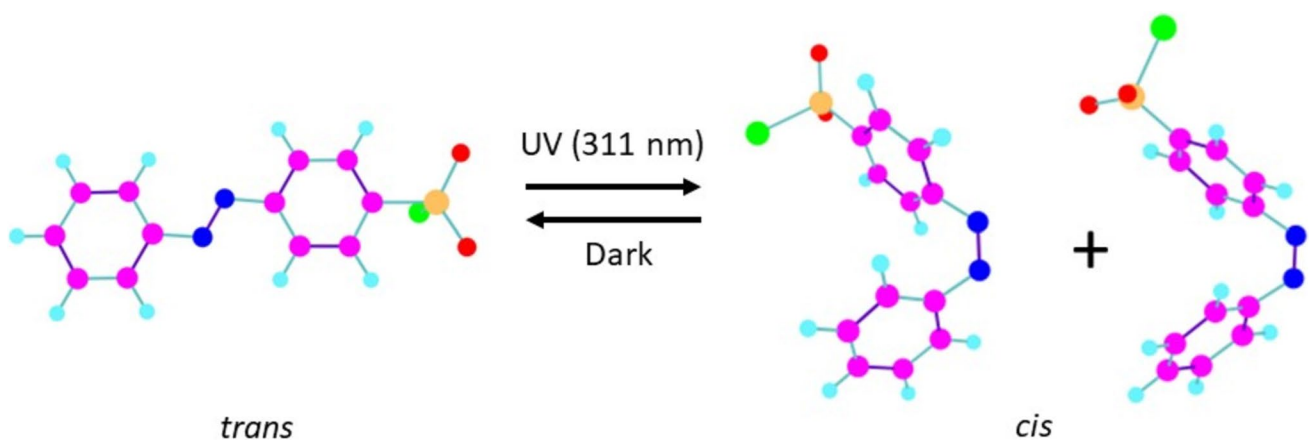

Keywords Azo dye · Photoisomerization · Reversal in solvatochromism · Photochemistry · Solvent effects · UV irradiation

Extended author information available on the last page of the article

Published online: 23 January 2025

1 Introduction

Azobenzene can exist in *trans* and *cis* isomeric forms, with the first being ~ 40–60 kJ mol^{-1} more stable than the latter [1–3]. The reversible *trans–cis* isomerization in azobenzene and its derivatives in solution has been extensively investigated, and found to be significantly influenced by the solvent properties, including polarity and H-bonding ability, as well as by specific characteristics of the substituents present in the aromatic rings [1–9]. Nevertheless, no single mechanism can satisfactorily explain all aspects of the isomerization process in azobenzenes, even for the unsubstituted parent compound, so that this is still a topic of current research [3]. *Trans*-to-*cis* isomerization in azobenzenes may occur upon excitation with ultraviolet (UV) light [1, 2, 4, 5], mechanical stress [6], or electrostatic excitation [7, 8], while easy thermal *cis* → *trans* isomerization is in general observed due to the usual low thermodynamic stability of the *cis* isomer [4, 5, 9]. Besides *trans–cis* isomerization, azobenzene exhibits remarkable photostability, with negligible decomposition occurring even after prolonged UV irradiation [3].

Azobenzenes are substances exhibiting colors that cover the whole visible spectrum. In these compounds, the azo bond (-N = N-) brings the two aromatic systems into conjugation, leading to an extended system of delocalized π-electrons whose specific electronic properties depends on the substituents present in the rings and their positions [10]. The electronic spectra of the *cis* and *trans* isomers are also distinctive [11, 12].

The photochromic properties of the azobenzene moiety have been used as a light-triggered switch in various polymers [13–15], surface-modified materials [16–18], protein probes [19–22], molecular machines [23–25], holographic recorders [26–28] and metal ion chelators [29–32]. The change in geometry following isomerization directs molecules to perform a function [33–35], modulates interactions that alter the structure of the bulk material [36–38], changes spectroscopic properties [39–41], or moves a substituent that blocks or unblocks activity [20, 42–44]. Azobenzene motif is also used as a chromophore in various pH [45, 46] and metal ion indicators [47, 48], as well as in the production of industrial dyes and nonlinear optical devices [49].

The electronic properties of a compound, including its absorbance spectrum, are influenced by the solvent characteristics. Solvatochromism is indeed a convenient and simple method to interpret solute–solvent interactions [50, 51], and to obtain information on specific characteristics of the relevant electronic states of the solute, since the solvatochromic effects may affect differently the different electronic states [52].

The present study focused on the solvatochromism exhibited by azobenzene-4-sulfonyl chloride (abbreviated as Azo-SCl) in a series of non-polar (hexane, heptane, cyclohexane, 1,4-dioxane, benzene, toluene, diethyl ether), polar-aprotic (chloroform, n-butyl acetate, chlorobenzene, ethyl acetate, dichloromethane, acetonitrile, dimethyl formamide, dimethyl sulfoxide) and polar-protic (1-octanol, 1-butanol, 2-propanol, ethanol, methanol, ethylene glycol) solvents. Ultraviolet–visible (UV–vis) absorbance spectroscopy has been selected as probing technique. Azo-SCl is expected to show interesting solvatochromic behavior because it carries the sulfonyl chloride moiety, which is able to establish different types of interactions with the solvent. The SO_2Cl substituent is a deactivating group and tends to pull the electron density towards the ring. This group tends to interact with solvent through dipole–dipole interactions and is also expected to possess a strong H-bond acceptor ability due to the S = O group it carries. Therefore, the effect of this substituent on the solvatochromic behavior and photoisomerization properties of the parent azobenzene molecule appeared of interest to further our understanding of azobenzenes' physical chemistry. The solvent effects have been evaluated by applying the multiparametric Catalán and Kamlet-Taft solvatochromic models. In addition, photoisomerization of Azo-SCl upon UV irradiation ($\lambda \geq 311$ nm) was studied in all investigated solvents. Interpretation of the experimental data is supported by quantum chemical calculations undertaken within the Density Functional Theory framework.

2 Materials and instruments

Azobenzene-4-sulfonyl chloride (> 98%) was purchased from TCI and used without any further purification. All solvents were obtained high purity (spectroscopic grade) from Sigma-Aldrich. The concentrations of solutions were kept as low as possible ($< 5 \times 10^{-5}$ M) in order to avoid aggregation of the compound. The UV–vis spectra were obtained in the 190–800 nm wavelength range using a Schimadzu UV–Vis spectrophotometer UV-2600i. All measurements were performed using a quartz cell (standard cell, with 1 cm × 1 cm optical path), at room temperature, and after the solutions were kept in the dark for five days after preparation. The wavelengths of the band maxima were determined after band deconvolution, performed using OriginPro 2021 [53] and UVProbe spectroscopy (version 2.71) (SHIMADZU) software. In the photoisomerization experiments, the solutions were exposed to radiation provided by a broad-band 18 W UV source ($\lambda \geq 311$ nm). Irradiation was first performed during 1 min and then in consecutive series of 5 min, the UV–vis spectrum of the sample being recorded after each irradiation period in order to follow the progress of the photoreaction.

3 DFT calculations

All calculations were carried out at the DFT/B3LYP level of theory, with the 6–311 + +G(d,p) basis set [54–59], using GAUSSIAN 09 (revision C.01) [60]. Possible isomeric structures of the investigated azobenzene were subjected to geometry optimization in their electronic ground states, and their relative energies and vibrational frequencies were calculated. The frequency calculations were performed to confirm that the optimized geometries correspond to true minima. Excited state calculations were done within the time-dependent DFT (TD-DFT) theoretical framework [61, 62], the UV–vis spectra being calculated using the same functional and basis set as for the ground state calculations. For representation of the calculated UV–vis data, a scale factor of 0.92 (adjusted by fit of the calculated to experimental data) was used in order to allow for a better comparison between the experimental data and the theoretical predictions. The GaussView 5.0 [63] and ChemCraft (version 1.8) [64] programs were used both for the preparation of input files and visualization of the results.

4 Results and discussion

4.1 Structural and energetical characterization of the cis and trans Azo-SCl isomers

A conformational search on the potential energy surface of the two isomers of Azo-SCl revealed that the *cis* form has two different conformers differing in the orientation of the SO_2Cl group (*cis*1 and *cis*2 forms; see Fig. 1), while in the case of the *trans* isomer only one conformer was located. All forms are C_1 symmetry and have a symmetry-equivalent form. The calculations show that the *trans* isomer is ~ 62 kJ mol^{-1} lower in energy than both *cis*1 and *cis*2 forms, which are nearly degenerate (the energy difference between *cis*1 and *cis*2 is only 0.4 kJ mol^{-1}, indicating that the different orientation of the SO_2Cl substituent with respect to the ring plane does not causes a significant change in energy). In parent azobenzene, the *trans–cis* energy difference has been reported as 64.2 kJ mol^{-1} [65]. Similar values have also been reported for other azobenzenes, such as azobenzene-4-hydroxy (69.5 kJ mol^{-1}), azobenzene-4-(2-hydroxy)ethanol (66.2 kJ mol^{-1}) or azobenzene-4-dimethylamine-4´-sulfonylamide (69.8 kJ mol^{-1}) [65].

In *trans* Azo-SCl, the C_1-N_1 = N_2-C_7 dihedral angle is ~ 180° (± 179.8°, the signal + or – referring to the value of the angle in each one of the two equivalent-by-symmetry minima), whereas in both *cis*1 and *cis*2 conformers this angle is ~ 10° (± 9.4° and ± 9.5° in *cis*1 and *cis*2, respectively). The orientation of the SO_2Cl substituent in both *trans* and *cis* isomers is such that the chlorine atom stays nearly perpendicular to the ring, allowing for hyperconjugation with the ring π system, and additional stabilizing C–H···O = S interactions are also present in all forms, the H···O distances being calculated as ~ 2.591 – 2.601 Å. The arrangement of the SO_2Cl group is similar to that observed experimentally for benzene sulfonyl chloride [66], where refinement of the gas phase electron diffraction data was compatible with two models where the angle formed by the S–Cl bond and the ring plane is either 73.5 or 90.0º, the H···O distances being slightly longer than those calculated for Azo-SCl (*ca.* 2.631 Å) [66] (Table 1).

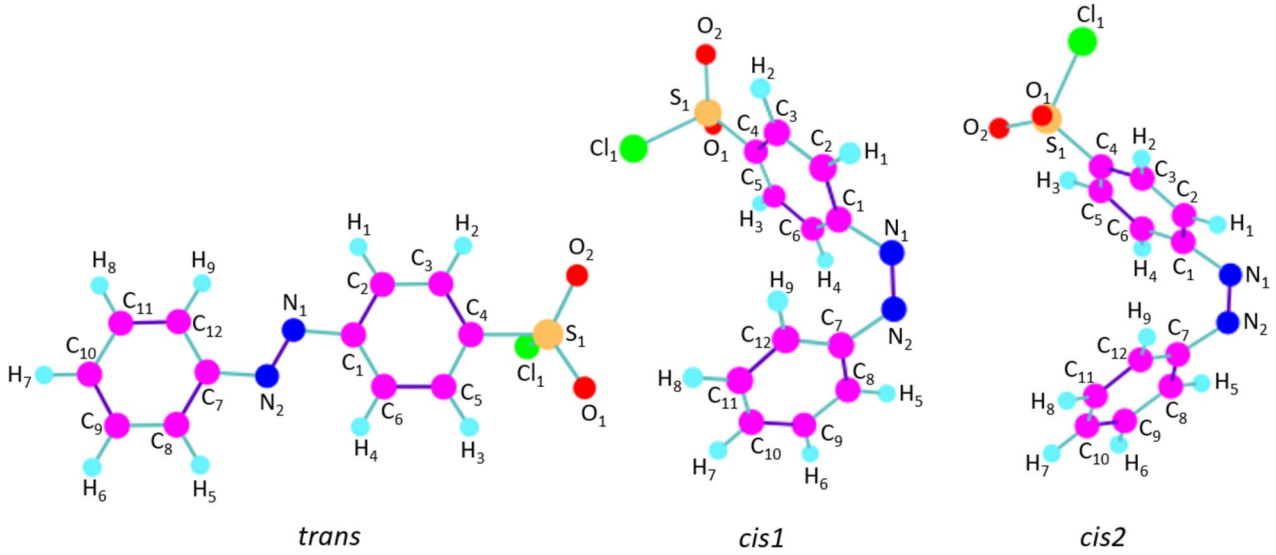

Fig. 1 Relevant DFT(B3LYP)/6–311 + +G(d,p) optimized minimum energy structures for Azo-SCl isomers

Table 1 B3LYP/6–311 + + G(d,p) calculated geometrical parameters, relative electronic energies (ΔE_{el}), zero-point corrected electronic energies (ΔE_0) and standard Gibbs energies (ΔG^0_{298K}) for *trans* and *cis* forms of Azo-SCl[a]

	trans	*cis1*	*cis2*	Exp. [66][b]
ΔE_{el}/kJ mol^{-1}	0	62.5	62.8	
ΔE_0/kJ mol^{-1}	0	62.0	62.3	
ΔG^0/kJ mol^{-1}	0	63.7	63.9	
$\phi C_1\text{-}N_1=N_2\text{-}C_7$/°	− 179.8	− 9.4	− 9.5	
$\phi Cl_1\text{-}S_1\text{-}C_4\text{-}C_3$; $\phi Cl_1\text{-}S_1\text{-}C_4\text{-}C_5$/°	− 90.9; 89.7	− 90.8; 90.3	− 90.2; 89.8	75.3 ± 5.0 or 90.0[c]
$\theta Cl_1\text{-}S_1=O_2$; $\theta Cl_1\text{-}S_1=O_1$/°	106.0; 105.9	105.8; 105.8	105.9; 105.9	105.5 ± 1.8
$\theta O_1=S_1=O_2$/°	122.3	122.4	122.3	122.5 ± 3.6
$\theta C_4\text{-}S_1=O_1$; $\theta C_4\text{-}S_1=O_2$/°	109.7;109.7	109.7;109.7	109.6;109.6	110.0 ± 2.5
$\theta C_4\text{-}S_1\text{-}Cl_1$ / °	100.8	100.9	101.2	100.9 ± 2.0
$rO_2\cdots H_2$; $rO_1\cdots H_3$/Å	2.591; 2.598	2.593; 2.592	2.596; 2.601	2.631
$rS_1=O_1$; $rS_1=O_2$/Å	1.451; 1.451	1.451; 1.451	1.451; 1.451	1.417 ± 0.012
$rS_1\text{-}Cl_1$/Å	2.144	2.147	2.143	2.047 ± 0.008
$rS_1\text{-}C_4$/Å	1.787	1.783	1.783	1.764 ± 0.009

[a]For structures, see Fig. 1

[b]Experimental data (gas phase electron diffraction) for benzene sulfonyl chloride [66]

[c]Two alternative refinement models were reported in [66]

4.2 Solvatochromism – UV–vis spectra of Azo-SCl in different solvents

Solid Azo-SCl ($C_{12}H_9ClN_2O_2S$, $M = 280.73$ g mol^{-1}) is matte brown toned red powder in appearance. The solutions of the compound are yellow in all solvents studied, appearing lighter in non-polar solvents due to the reduced solubility of the compound in these solvents.

The UV–vis absorption spectra of Azo-SCl in solutions of non-polar, polar-aprotic, and polar-protic solvents are depicted in Figs. 2, 3 and 4, respectively. The two longest wavelength bands are observed in the 321–330 nm (band-I; λ_{max}^{I}) and 435–461 nm (band-II; λ_{max}^{II}) ranges. As for parent azobenzene [9, 67–71], band-I can be attributed to the π*- π ($S_2 \leftarrow S_0$) transition and band-II to the π*-n ($S_1 \leftarrow S_0$) transition, though the SO_2Cl substituent in Azo-SCl leads to red-shifts of ~ 10 nm in the two bands compared to the corresponding bands of parent azobenzene.

In the studied non-polar solvents (solvents 1 to 7; see Table 2) λ_{max}^{I} and λ_{max}^{II} are observed between 323 and

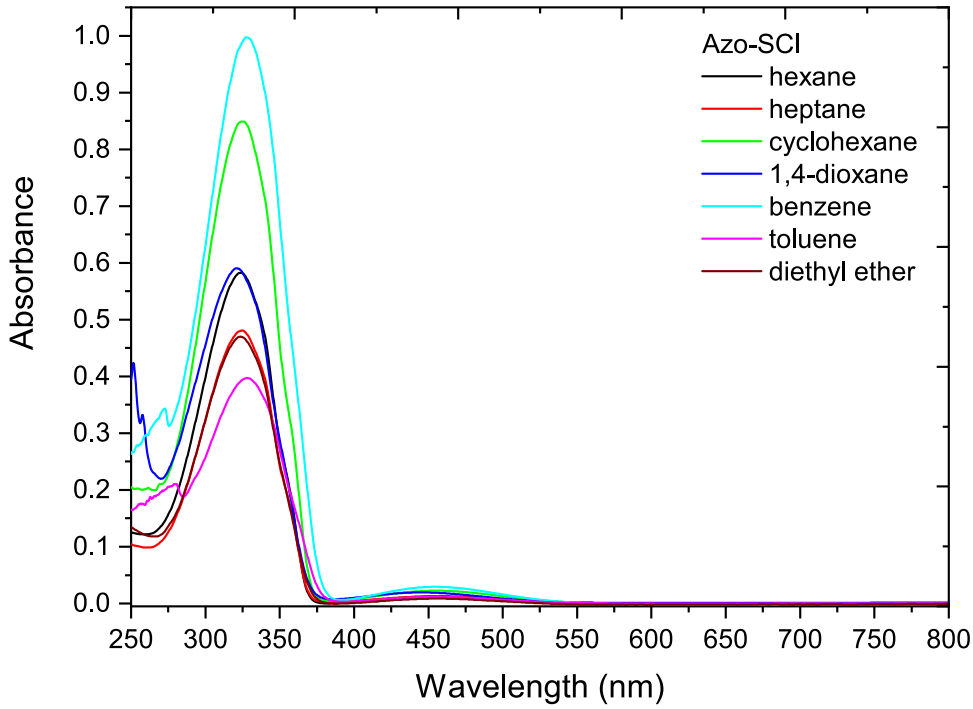

Fig. 2 UV–vis absorption spectra of the Azo-SCl molecule in non-polar solvents

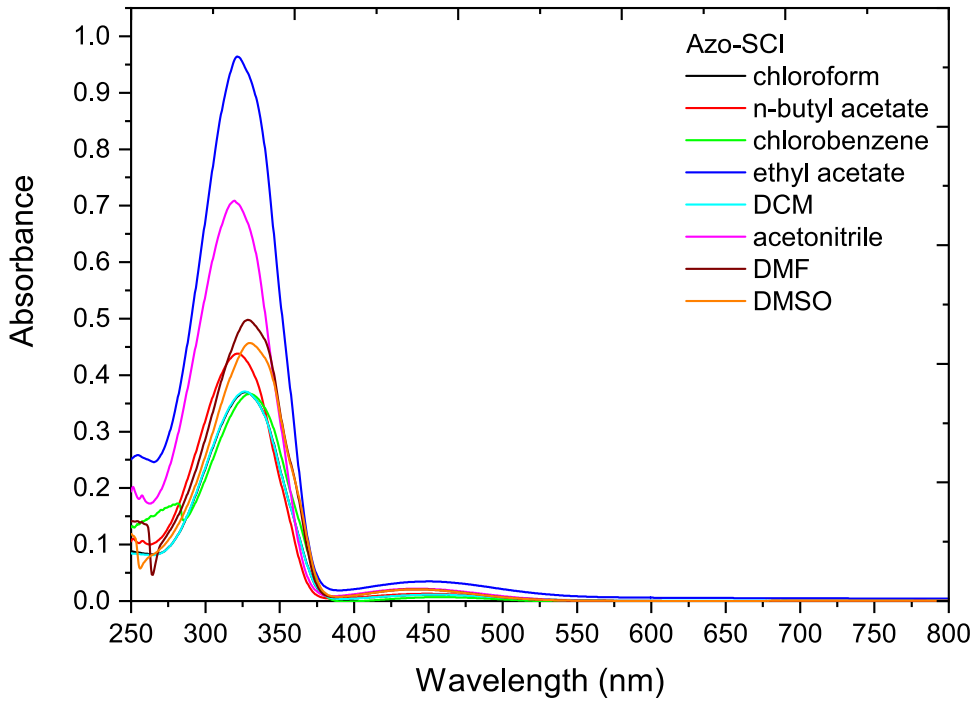

Fig. 3 UV–vis absorption spectra of the Azo-SCl molecule in polar-aprotic solvents

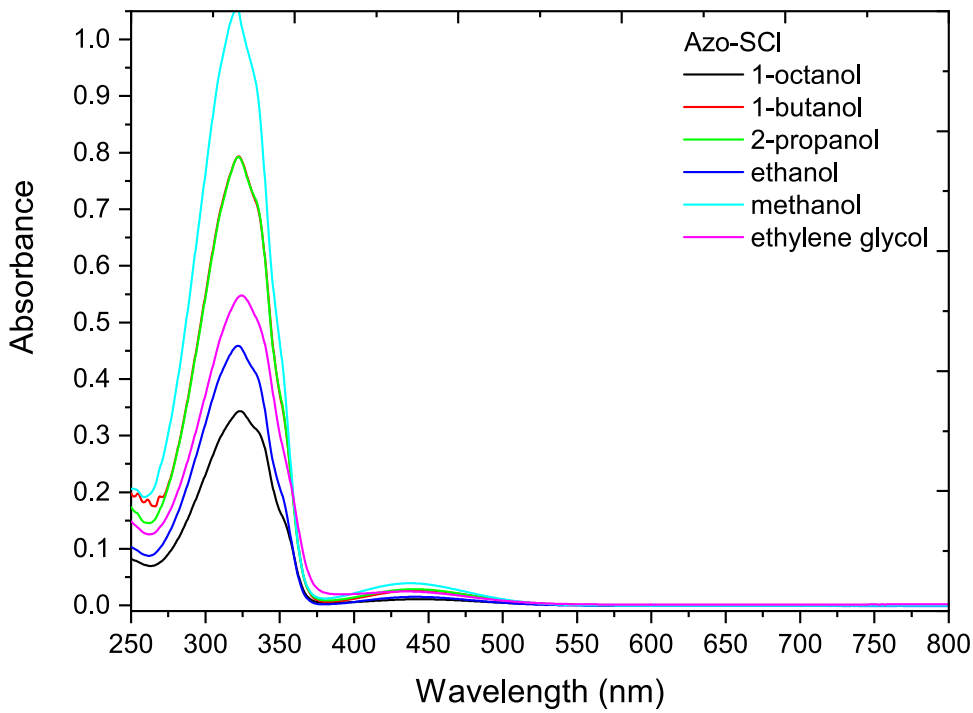

Fig. 4 UV–vis absorption spectra of the Azo-SCl molecule in polar-protic solvents

328 nm and between 448 and 461 nm, respectively, with a trend to red shift with the increase of solvent dielectric constant (ε), this shift being more noticeable for λ_{max}^{I}, which globally shows a stronger dependence on the solvent.

For the majority of the polar-aprotic solvents investigated (8–12, 18, 19, 21), λ_{max}^{I} is observed nearly in the same range as for the non-polar solvents, 322–330 nm, exhibiting a red shift of ~ 8 nm in going from the least polar solvents (ethyl acetate/acetonitrile) to the most polar one (DMSO). In turn, in the studied polar-aprotic solvents λ_{max}^{II} is observed within the range 442–450 nm, but contrarily to λ_{max}^{I} it exhibits a general blue shift (of ca. –7 nm) in going from the least to the most polar aprotic solvent.

Table 2 Solvent dielectric constant (ε), wavelengths (λ_{max}) of band-I and band-II and wavenumbers ($_{max}$) extracted from wavelengths and calculated by Catalán and Kamlet-Taft multiparametric models

No	Solvent	ε	band-I λ_{max}^{I} (nm)	band-I ν_{max}^{I} (cm^{-1})	band-I ν_{max}^{I} (cm^{-1}) Catalán	band-I ν_{max}^{I} (cm^{-1}) Kamlet-Taft	band-II λ_{max}^{II} (nm)	band-II ν_{max}^{II} (cm^{-1})	band-II ν_{max}^{II} (cm^{-1}) Catalán	band-II ν_{max}^{II} (cm^{-1}) Kamlet-Taft
1	Hexane	1.88	323.5	30,912	30,980	30,887	454	22,026	21,890	21,841
2	Heptane	1.92	324.5	30,817	30,930	30,907	454	22,026	21,895	21,825
3	Cyclohexane	2.02	324.5	30,817	30,798	30,868	455	21,978	21,896	21,856
4	1,4-dioxane	2.21	324.5	30,817	30,660	30,676	448	22,321	22,087	22,178
5	Benzene	2.27	327.5	30,534	30,491	30,602	454.5	22,002	22,028	22,118
6	Toluene	2.38	328	30,488	30,521	30,628	455.5	21,954	22,034	22,101
7	Diethyl ether	4.20	323.5	30,912	30,992	30,831	460.5	21,716	22,128	22,096
8	Chloroform	4.89	327	30,581	30,522	30,728	450	22,222	22,210	22,295
9	*n*-butyl acetate	5.07	324.5	30,817	30,829	30,735	452	22,124	22,192	22,165
10	Chlorobenzene	5.62	330	30,303	30,377	30,538	457	21,882	22,155	22,157
11	Ethyl acetate	6.02	322.5	31,008	30,877	30,692	450.5	22,198	22,223	22,201
12	DCM	8.93	326	30,675	30,580	30,532	450	22,222	22,286	22,271
13	1-octanol	10.30	323.5	30,912	30,853	31,084	445.5	22,447	22,465	22,608
14	1-butanol	17.51	322.5	31,008	30,963	31,071	443.5	22,548	22,570	22,665
15	2-propanol	19.92	322	31,056	31,050	31,070	440.5	22,701	22,589	22,675
16	Ethanol	24.55	322	31,056	31,084	31,028	442	22,624	22,653	22,681
17	Methanol	32.66	321	31,153	31,216	31,001	438	22,831	22,862	22,710
18	Acetonitrile	35.94	322.5	31,008	30,898	30,628	446	22,422	22,387	22,331
19	DMF	36.71	328.5	30,441	30,599	30,580	442.5	22,599	22,428	22,399
20	Ethylene glycol	37.70	324.5	30,817	30,793	30,816	435.5	22,962	22,967	22,794
21	DMSO	46.45	330	30,303	30,420	30,536	442	22,624	22,482	22,466

In the case of polar-protic solvents (13–17,20), λ_{max}^{I} is within the 321–325 nm range, whereas λ_{max}^{II} stays in the range of 435–446 nm and shows a maximum blue shift of ca. 11 nm for ethylene glycol (compared to 1-octanol).

The λ_{max} values obtained from the UV absorption spectra in the different solvents are plotted as a function of the solvent dielectric constant ε in Fig. 5. The plot for band-1 (Fig. 5a) highlights a reversal in solvatochromism: in going from the non-polar solvents to methanol (ε = 32.66), the

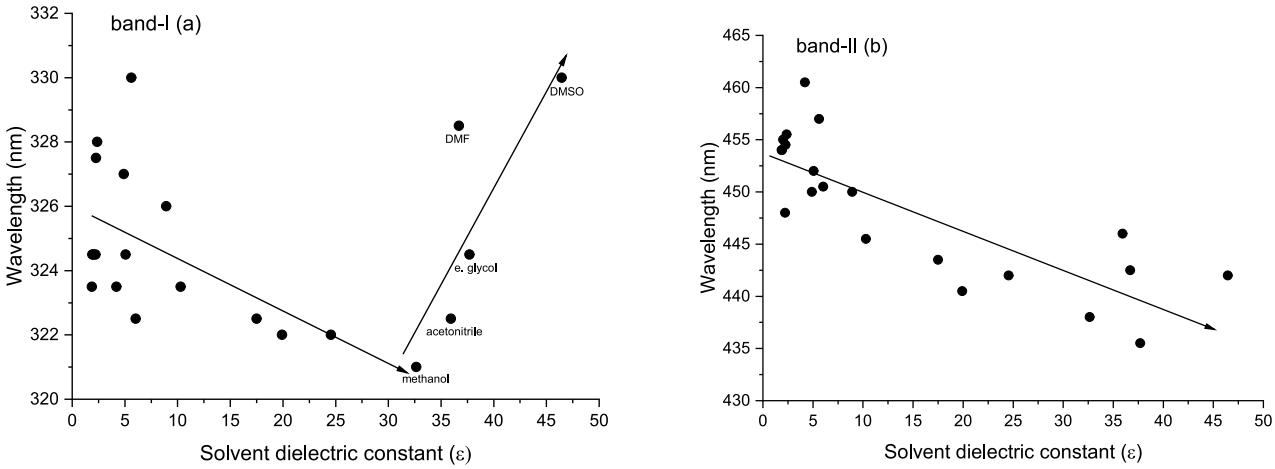

Fig. 5 Plots of maximum absorption wavelength of band-I (a) and band-II (b) *versus* dielectric constant of the solvent

λ_{max}^{I} values decrease from ca. 328–324 to 321 nm with the increase of the polarity of the solvent (negative solvatochromism), while in going from methanol to DMSO (ε = 46.45) the λ_{max}^{I} values increase from 321 to 330 nm (positive solvatochromism). Thus, band-I of Azo-SCl exhibits a general negative solvatochromism for solvents with ε values in the 1.88–32.66 range, and positive solvatochromism for solvents with ε values higher than 32.66, the reversal occurring at an ε value of 32.66, which is characteristic of methanol. On the other hand, λ_{max}^{II} values indicate a general negative solvatochromism in all range of solvent's dielectric constant investigated (Fig. 5b). The distinct solvatochromic behavior of band-I and band-II demonstrate different interactions of Azo-SCl with the different solvents in its S_2 and S_1 excited states.

4.3 Solvatochromism in Azo-SCl at the light of the Catalán and Kamlet-Taft multiparametric models

In order to shed light on the solute–solvent interactions effects on the $S_1 \leftarrow S_0$ and $S_2 \leftarrow S_0$ transitions of Azo-SCl, Kamlet-Taft [72–75] and Catalán [52, 76] multiparametric models were applied to the obtained spectroscopic data. These models obey empirical relations given by Eqs. 1 and 2, respectively:

$$\nu_{max} = \nu_0 + a(\alpha) + b(\beta) + p(\pi *) \quad (1)$$

$$\nu_{max} = \nu_0 + a_{SA}(SA) + b_{SB}(SB) + d_{SP}(SP) + e_{SdP}(SdP) \quad (2)$$

where ν_0 is the wavenumber corresponding the λ_{max} value for a solvent-unaffected solute, and a, b, p, a_{SA}, b_{SB}, d_{SP} and e_{SdP} are coefficients that reflect the contribution of the different solvent parameters to the ν_{max} values determined from the observed band positions in the different solvents. The Kamlet-Taft model uses three parameters related with the hydrogen bonding acceptor (HBA) and hydrogen bonding donor (HBD) capabilities, and dipolarity/polarizability of a solvent, α, β and π*, respectively, while the Catalán model uses four parameters, SA, SB, SP and SdP, which are related with the solvent acidity, basicity, polarizability and dipolarity, respectively (Table 3).

Application of the Kamlet-Taft and Catalán models to the ν_{max}^{I} and ν_{max}^{II} experimental data for Azo-SCl yields the results given in Table 4. Figure S1, provided in the Supporting Information, shows the plots of the calculated ν_{max}^{I} and ν_{max}^{II} values for band-I and band-II using the developed models as a function of the experimental ν_{max}^{I} and ν_{max}^{II} values, whose R^2 values for linear fittings demonstrate the good agreement between the calculated and experimental data, with the Catalán model providing slightly better results (in particular in the case of band-I).

Table 3 Dielectric constants (ε), and Kamlet-Taft and Catalán solvent parameters for the used solvents [48, 63, 67, 68]

No	Solvent	ε	Catalán parameters				Kamlet-Taft parameters		
			SA	SB	SP	SdP	α (HBD)	β (HBA)	π*
1	hexane	1.89	0.000	0.056	0.616	0.000	0.00	0.00	− 0.04
2	heptane	1.94	0.000	0.083	0.635	0.000	0.00	0.00	− 0.08
3	cyclohexane	2.02	0.000	0.073	0.683	0.000	0.00	0.00	0.00
4	1,4-dioxane	2.21	0.000	0.444	0.737	0.312	0.00	0.37	0.55
5	benzene	2.27	0.000	0.124	0.793	0.270	0.00	0.10	0.59
6	toluene	2.38	0.000	0.128	0.782	0.284	0.00	0.11	0.54
7	diethyl ether	4.20	0.000	0.562	0.617	0.385	0.00	0.47	0.27
8	chloroform	4.89	0.047	0.071	0.783	0.614	0.44	0.00	0.58
9	*n*-butyl acetate	5.07	0.000	0.525	0.674	0.535	0.00	0.45	0.46
10	chlorobenzene	5.62	0.000	0.182	0.833	0.537	0.00	0.07	0.71
11	ethyl acetate	6.02	0.000	0.542	0.656	0.603	0.00	0.45	0.55
12	DCM	8.93	0.040	0.178	0.761	0.769	0.13	0.10	0.82
13	1-octanol	10.30	0.299	0.923	0.713	0.454	0.77	0.81	0.40
14	1-butanol	17.51	0.341	0.809	0.674	0.655	0.79	0.88	0.47
15	2-propanol	19.92	0.283	0.830	0.633	0.808	0.76	0.95	0.48
16	ethanol	24.55	0.400	0.658	0.633	0.783	0.83	0.77	0.54
17	methanol	32.66	0.605	0.545	0.608	0.904	0.93	0.62	0.60
18	acetonitrile	35.94	0.044	0.286	0.645	0.974	0.19	0.31	0.75
19	DMF	36.71	0.031	0.613	0.759	0.977	0.00	0.69	0.88
20	ethylene glycol	37.70	0.717	0.534	0.777	0.910	0.90	0.52	0.92
21	DMSO	46.45	0.072	0.647	0.830	1.000	0.00	0.76	1.00

Table 4 Multilinear regression coefficients obtained using the Catalán and Kamlet-Taft solvatochromic models for the $S_1 \leftarrow S_0$ and $S_2 \leftarrow S_0$ transition of Azo-SCl as observed in the UV–vis absorbance spectra

Dye analysis	Band-I (ν_{max}^{I}) Catalán	Band-II (ν_{max}^{II}) Catalán	Dye analysis	Band-I (ν_{max}^{I}) Kamlet-Taft	Band-II (ν_{max}^{II}) Kamlet-Taft
ν_0	32,662.1 ± 225.9	21,846.7 ± 381.7	ν_0	30,867.8 ± 87.5	21,856.2 ± 84.1
a_{SA}	358.3 ± 123.4	841.8 ± 208.6	a	321.7 ± 133.4	474.4 ± 132.4
b_{SB}	52.0 ± 101.9	136.7 ± 172.2	b	200.4 ± 161.4	281.8 ± 160.2
–	–	–	p	− 484.4 ± 144.7	395.7 ± 143.7
d_{SP}	− 2735.3 ± 317.2	58.3 ± 535.9	–	–	–
e_{SdP}	− 30.8 ± 87.9	437.7 ± 148.4	–	–	–
N	21	21	N	21	21
R	0.940	0.904	R	0.758	0.877
R^2	0.883	0.817	R^2	0.574	0.769
F	30.304	17.810	F	7.643	18.838
P	0.000	0.000	P	0.002	0.000

It shall be noted that the relative modest fit between the experimental and calculated data resulting from the models may indicate that non-linear effects resulting from synergistic (positive or negative) effects between the different solvent–solute interaction types are relatively important in for the studied solute in some of the solvents investigated.

As seen from Table 4, the magnitudes of the coefficients estimated from Catalán model vary in the order $d_{SP} > a_{SA} > b_{SB} > e_{SdP}$ for band-I (π*-π, $S_2 \leftarrow S_0$) and $a_{SA} > e_{SdP} > b_{SB} > d_{SP}$ for band-II (π*-n, $S_1 \leftarrow S_0$). In the case of the Kamlet-Taft model, the magnitude of the parameters follows the order $p > a > b$ for band-I, and $a > p > b$ for band-II. It can then be concluded that both models predict that the solvent HBD ability (affected by the a and a_{SA} coefficients in the models' equations) has a larger contribution to ν_{max}^{I} and ν_{max}^{II} than the solvent HBA ability (affected by b and b_{SB} coefficients), with both solvent parameters resulting in a wavenumber shift to higher values (wavelength shift to lower values; bathochromic shift). The Catalán model predicts that the effect of solvent polarizability (as measured by the coefficient d_{SP}) on band-I is ~ 47 times larger than on band-II, being of opposite sign, while the effect of dipolarity (measured by the value of the e_{SdP} coefficient) is ~ 15 times smaller and also of opposite sign. Polarizability and dipolarity effects lead to a reduction of ν_{max}^{I} and to an increase of ν_{max}^{II} (hypsochromic and bathochromic shifts in wavelengths, respectively). It is significant to point out that the Catalán model predicts the solvent polarizability as the most effective solvent property in determining the spectral shifts of band-I, followed by a relatively smaller contribution of solvent HBD ability, while spectral shifts of band-II are dominated mostly by solvent acidity alongside a smaller contribution of dipolarity.

In agreement with the Catalán model, the Kamlet-Taft model also indicates that the contributions of the polarizability/dipolarity of the solvent to ν_{max}^{I} and ν_{max}^{II} (as measured by the coefficient p) have opposite sign, leading to a reduction of ν_{max}^{I} and to an increase of ν_{max}^{II}.

As seen from the sign of the estimated parameters (negative d_{SP}, e_{SdP} and positive a_{SA}, b_{SB} in Catalán model; negative p and positive a an b in Kamlet-Taft model) presented in Table 4, the observed reversal in the solvatochromic behavior of band-I ($S_2 \leftarrow S_0$) can then be assigned to the opposite effects of solvent dipolarity/polarizability and hydrogen bonding ability on S_2, the first stabilizing and the second destabilizing this excited state in relation to the ground state. When taken together, these effects explain the observed bathochromic shifts of band-I in solvents such as acetonitrile, DMF, ethylene glycol and DMSO as a consequence of their high polarity, while the hypsochromic shifts observed in for the remaining solvents result from the moderate/weak HBA and HBD effects of the solvents. On the other hand, dipolarity/polarizability and hydrogen bonding ability of the solvents act synergically in the case of S_1 (both destabilizing the excited state) leading to the general negative (hypsochromic) solvatochromism exhibited by band-II. We shall turn to this subject in the next section.

The maximum wavelengths of solvent-unperturbed bands (ν_0 values) estimated by Catalán and Kamlet-Taft models are 306 ± 2 and 324 ± 1 nm (for band-I) and 458 ± 2 nm (for band-II; both models). Though for band-I the ν_0 values predicted by the models differ in some amount, they point to occurrence of an hypsochromic shift in going from the gas phase to solution, while both models indicate that band-II undergoes a bathochromic shift. These results are also a clear indication of the different solvent interactions with the S_1 and S_2 solute states and their effects on the $S_1 \leftarrow S_0$ and $S_2 \leftarrow S_0$ transition energies along the series of the studied solvents.

4.4 UV-induced photoisomerization and S_1 and S_2 excited states of the isomers of Azo-SCl

The UV–vis absorption spectra of the three forms of Azo-SCl were calculated at the TD-DFT/B3LYP/6–311 + + G(d,p) level, in the gas phase. The simulated spectra are shown in Fig. 6 and the results are summarized in Table 5. The results of these calculations show a good general agreement with data obtained using the same basis set and the range-separated functional CAM-B3LYP [77], which is known to be generally more reliable to take into account charge/transfer transitions (Table S1 and Figure S2).

The TD-DFT/B3LYP/6–311 + + G(d,p) calculations predict the $S_1 \leftarrow S_0$ and $S_2 \leftarrow S_0$ transitions at 470.8 and 326.3 nm (B3LYP values scaled by 0.92; CAM-B3LYP: 471.2 and 319.6 nm) for *trans* Azo-SCl, at 454.7 and 327.8 nm for *cis1*, and at 452.9 and 326.9 nm for *cis2* (Table 2) (CAM-B3LYP: 469.8 and 281.8 for *cis1*, and 469.4 and 280.3 for *cis2*). In agreement with the observations, for the *trans* isomer, the $S_1 \leftarrow S_0$ transition was predicted by the calculations to have a very low oscillator strength ($f < 0.0001$), whereas the a $S_2 \leftarrow S_0$ transition has a large oscillator strength ($f = 0.8365$, B3LYP calculated value; CAM-B3LYP: 0.9728). These data are also in agreement with the known experimental data for the parent azobenzene, where the *trans* isomer gives rise to an absorption spectrum exhibiting two well separated bands in the region above 300 nm [9, 67–71]: a strong UV band at ~ 315 nm ascribed to π*-π $S_2 \leftarrow S_0$ transition, and a very weak band in the visible region (at ~ 445 nm) assigned to the symmetry forbidden π*-n $S_1 \leftarrow S_0$ transition.

In the case of the *cis* isomer of Azo-SCl (both conformers), the TD-DFT calculations predicted the $S_1 \leftarrow S_0$ and $S_2 \leftarrow S_0$ transitions at wavelengths that do not differ very much from those predicted for the *trans* isomer, but in this case with oscillator strengths relatively large ($f > 0.05$) and nearly equal (see Table 5 and Table S1). This spectral profile is similar to that observed experimentally for the parent *cis* azobenzene, where the π*-π $S_2 \leftarrow S_0$ and π*-n $S_1 \leftarrow S_0$ bands were observed at 250–270 and ~ 450 nm, respectively, with relatively similar intensities [9, 70].

According to the calculations, the HOMO–1, HOMO, LUMO and LUMO + 1 are the orbitals contributing the most to the $S_1 \leftarrow S_0$ and $S_2 \leftarrow S_0$ transitions in *trans* and *cis* Azo-SCl. In the *trans* isomer, the B3LYP calculations predicts the $S_1 \leftarrow S_0$ as corresponding mostly to the HOMO → LUMO transition while the $S_2 \leftarrow S_0$ is dominated by the HOMO–1 → LUMO transition. These orbitals are represented in Tables 5. The HOMO orbital is an n-type orbital localized on the oxygen and chlorine atoms of the sulfonyl chloride substituent; the HOMO–1 is a π-type orbital distributed on the azomethine and the nearby located ring carbon–carbon bonds, and the LUMO is also a π-type orbital delocalized through the whole azobenzene fragment.

The CAM-B3LYP results invert the order of energies of the two highest energy occupied orbitals, so that the HOMO is now the p orbital and the HOMO–1 the n-type orbital, but the descriptions of the transitions are identical to those predicted by the BLYP calculations (see Table S1). These

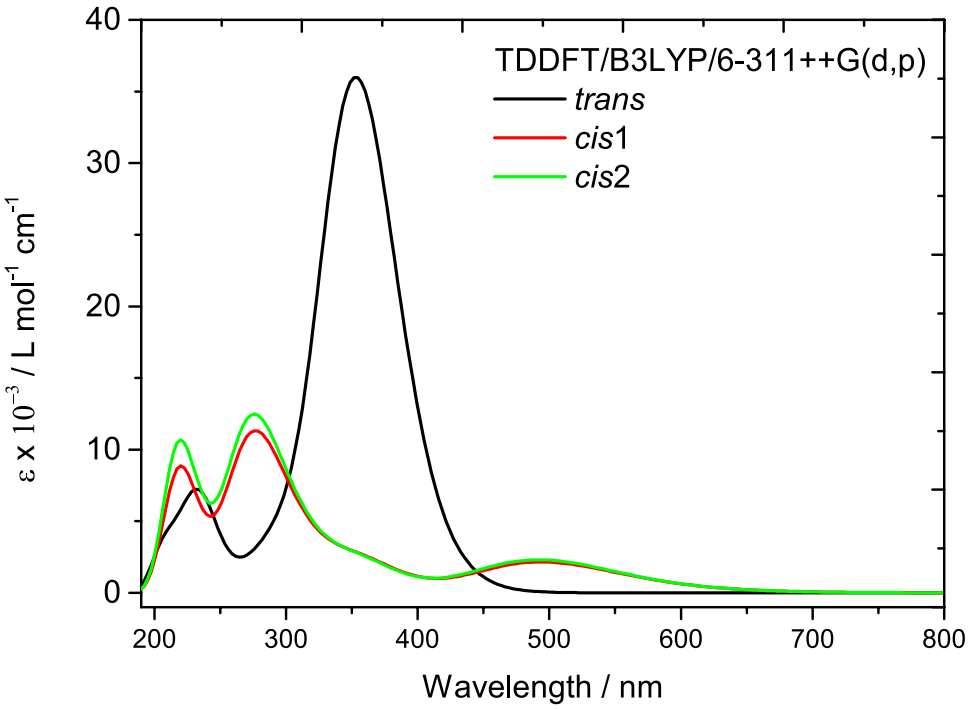

Fig. 6 TD-DFT/B3LYP/6–311 + + G(d,p) calculated UV–vis absorption spectra of *trans* and *cis* isomers of Azo-SCl. Wavelengths were scaled by 0.92

Table 5 TD-DFT/B3LYP/6–311 + +G(d,p) calculated lowest singlet excitation energies (λ, in nm; scaled by 0.92), oscillator strengths (f) and orbitals involved (with amplitudes in parenthesis) in the longest wavelength transitions for *trans* and *cis* isomers of Azo-SCl in the gas phase.

	State	λ	f	Major contribution	Donor orbital	Acceptor orbital
trans	S_1	470.8	0.0000	HOMO→LUMO (0.70)		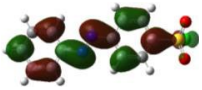
	S_2	326.3	0.8365	HOMO–1→LUMO (0.69)	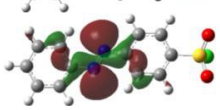	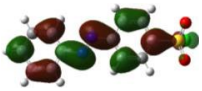
	S_3	306.3	0.0627	HOMO–2→LUMO (0.69)		
	S_4	287.2	0.0029	HOMO→LUMO+1 (0.68)		
	S_5	277.5	0.0265	HOMO–3→LUMO (0.67)		
cis1	S_1	454.7	0.0531	HOMO→LUMO (0.63) HOMO→LUMO+1 (–0.26)	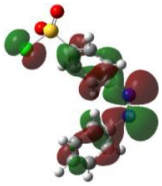 HOMO	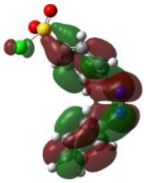 LUMO
	S_2	327.8	0.0545	HOMO→LUMO+1 (0.62) HOMO→LUMO (0.29)	 HOMO	 LUMO+1
	S_3	290.0	0.0161	HOMO–1→LUMO (0.67)		
	S_4	280.7	0.0650	HOMO–2→LUMO (0.64)		
	S_5	268.8	0.0016	HOMO→LUMO+2 (0.61) HOMO–4→LUMO+1 (0.32)		
cis2	S_1	452.9	0.0569	HOMO→LUMO (0.64) HOMO→LUMO+1 (0.26)	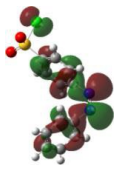 HOMO	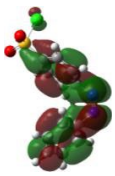 LUMO
	S_2	326.9	0.0536	HOMO→LUMO+1 (0.62) HOMO→LUMO (–0.29)	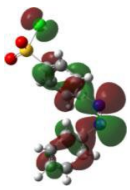 HOMO	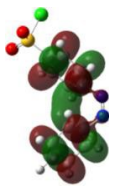 LUMO+1
	S_3	288.2	0.0220	HOMO–1→LUMO (0.67)		
	S_4	279.4	0.0657	HOMO–2→LUMO (0.64)		
	S_5	268.4	0.0019	HOMO→LUMO+2 (0.62) HOMO–4→LUMO+1 (0.31)		

results indicate that the $S_1 \leftarrow S_0$ transition has a high character of charge transfer from the sulfonyl chloride group to the azobenzene moiety, which should be highly sensitive to the polarizability/dipolarity of the solvent, and may be one of the major reasons for the different solvatochromic behavior observed for bands-I and II.

It shall also be pointed out that the $S_1 \leftarrow S_0$ and $S_2 \leftarrow S_0$ transitions in the *cis* Azo-SCl isomer have

similar major contributions in both *cis1* and *cis2* conformers, corresponding essentially to HOMO → LUMO and HOMO → LUMO + 1 transitions, respectively. In these forms, the HOMO, LUMO and LUMO + 1 orbitals have a predominant π-type character (justifying the appreciable intensity of the corresponding absorbance bands), the two first being delocalized over the whole azobenzene moiety and the last on the rings.

It has been shown that parent azobenzene *cis–trans* photoinduced interconversion can be triggered by pumping $S_1 \leftarrow S_0$ and $S_2 \leftarrow S_0$ transitions [4, 74]. In the present study, photoisomerization of Azo-SCl was investigated in all the 21 solvents used in this work (see Figure S2 in Supporting Information). Irradiation of the solutions was carried out at $\lambda \geq 311$ nm for 30 min as described in Sect. 2. Upon irradiation, noticeable changes in the relative intensities of band-I and band-II were observed, the first reducing of intensity and the second increasing. Observation of an isosbestic point (at ~ 389 nm) indicates that the observed reaction corresponds to a clean, two-component system without the formation of intermediate species. These results are consistent with occurrence of *trans*-to-*cis* isomerization. Notably, the photoisomerization starts promptly upon irradiation and a photostationary equilibrium state is fastly reached, confirming that the irradiation promotes the *trans–cis* photoisomerization in both directions. The photostationary state is solvent dependent being attained at different times of irradiation depending on the solvent, being tendentially reached faster for more polar solvents, as exemplified in Fig. 7 for chloroform (~ 30 min.), methanol (~ 20 min.), and DMSO (~ 5 min.).

For some representative solutions (heptane, chloroform, methanol and DMSO), the room temperature thermal conversion of the photogenerated *cis* isomer into the *trans* form was investigated by recording the UV–vis spectra of the solutions kept in dark after UV irradiation for 1 min (Fig. 8). In all the cases analyzed, it was found that band-I intensity rises while band-II intensity decreases after the storage of solution in the dark, in consonance with the conversion of the *cis* isomer into the *trans*. The changes completed in 1 min. in methanol and DMSO and in 5 min. in heptane and chloroform, demonstrating the fast room temperature decay of the higher energy *cis* isomer into the *trans* form, which appears to be also accelerated in more polar solvents.

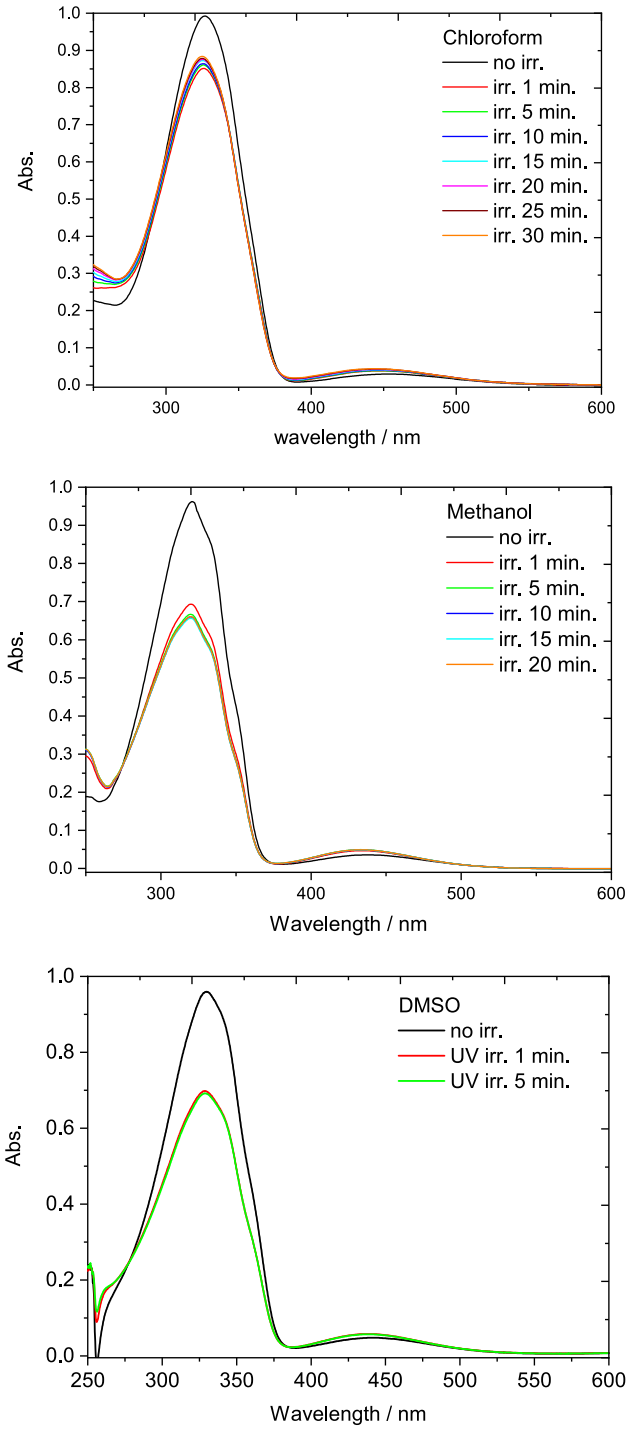

Fig. 7 Absorbance spectra of Azo-SCl in chloroform, methanol and DMSO solutions as a function of time (up to 30 min.) of UV irradiation ($\lambda \geq 311$ nm)

5 Conclusion

In this article, the solvatochromism of azobenzene-4-sulfonyl chloride (Azo-SCl) has been investigated in a series of non-polar, polar-aprotic, and polar-protic solvents. The UV–vis spectra of the compound exhibit two prominent long-wavelength absorption bands: one at 321–330 nm (band-I) and another at 435–461 nm (band-II). These bands were assigned to the π*-π ($S_2 \leftarrow S_0$) and π*-n ($S_1 \leftarrow S_0$) transitions, respectively.

A notable reversal in solvatochromism is observed for the shorter wavelength band (band-I), which shifts from

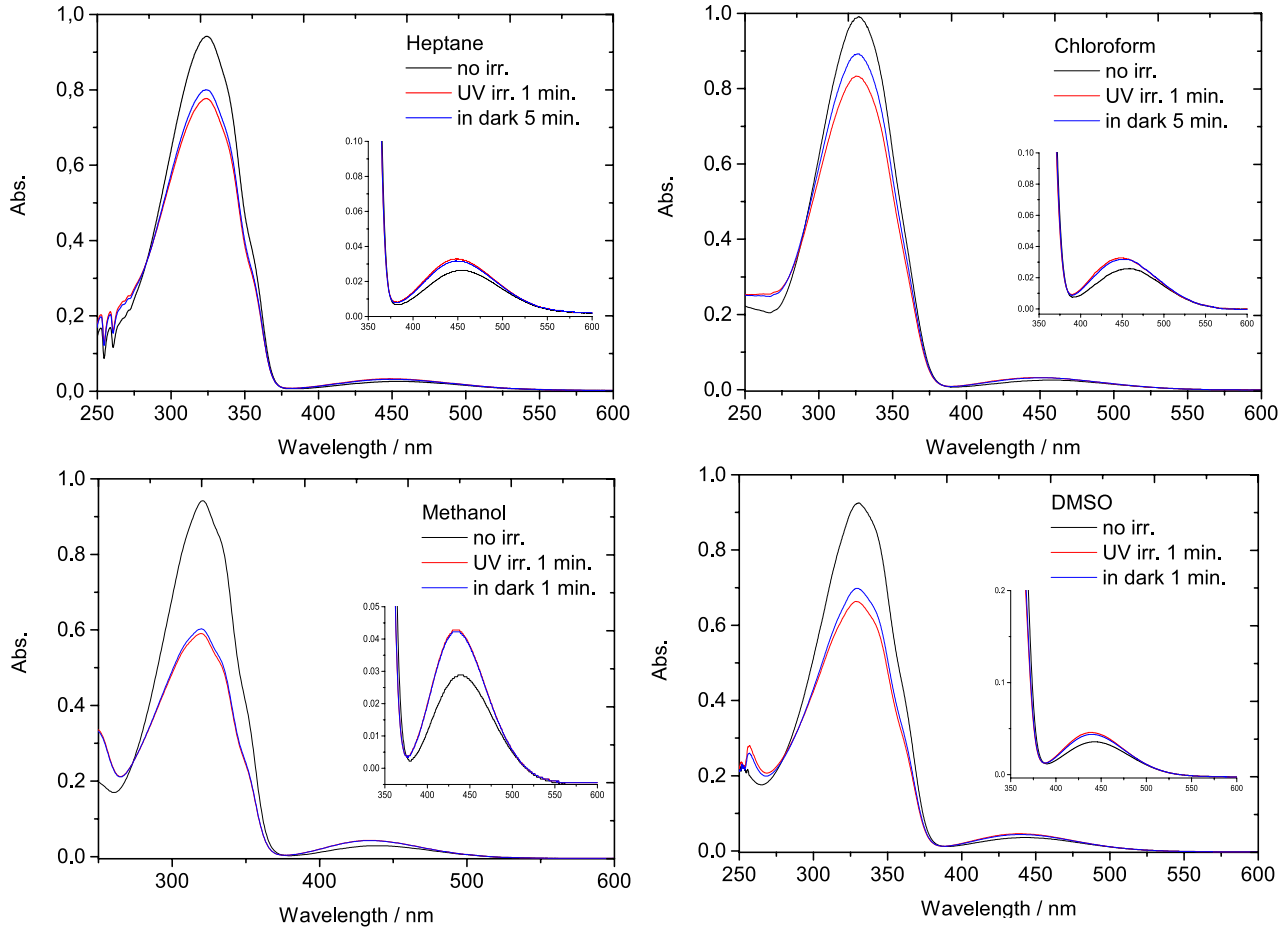

Fig. 8 UV–vis absorbance spectra of non-irradiated Azo-SCl in heptane, chloroform, methanol and DMSO solutions, of the samples irradiated during 1 min. ($\lambda \geq 311$ nm), and after subsequent storage in dark

negative to positive solvatochromism in solvents with a dielectric constant of around 32.66 (characteristic of methanol). In contrast, the longer wavelength band (band-II) exhibits negative solvatochromism across the entire range of solvent dielectric constants studied. This suggests different solvent interactions in the S_2 and S_1 excited states.

Using multiparametric Catalán and Kamlet-Taft solvation energy models, the reversal of solvatochromism in band-I ($S_2 \leftarrow S_0$) could be attributed to opposing effects of solvent dipolarity/polarizability and hydrogen bonding on the S_2 excited state. Solvent dipolarity/polarizability stabilizes this state, while hydrogen bonding destabilizes it relative to the ground state. In contrast, both factors act synergistically to destabilize the S_1 excited state, leading to consistent negative solvatochromism in band-II. These nuanced solvent interactions suggest that Azo-SCl can be finely tuned for specific responses, making it highly a versatile material.

Under UV irradiation ($\lambda \geq 311$ nm) at room temperature, Azo-SCl undergoes rapid *trans–cis* photoisomerization. In the absence of light, the photogenerated *cis* form quickly reverts to the more stable *trans* form. Both photoisomerization and thermal *cis* → *trans* thermal decay appear to be favored in more polar solvents. The rapid *trans–cis* photoisomerization under UV irradiation and the subsequent thermal *cis*-to-*trans* relaxation highlight Azo-SCl's potential in dynamic applications. The influence of solvent polarity on these processes further indicates that environmental conditions can modulate the compound's performance, offering adaptability for tailored functionalities in photoswitches, sensors, and molecular machines.

The interpretation of the experimental data was supported by quantum chemical calculations using Density Functional Theory (DFT), including Time-Dependent DFT for excited-state analysis.

Overall, the study bridges the gap between fundamental photophysics and practical applications, demonstrating how Azo-SCl's sensitivity to intermolecular interactions and reversible isomerization make it a promising candidate for advanced technologies. By leveraging these properties, Azo-SCl could play a pivotal role in the development of

responsive materials that depend on precise control over molecular states.

Supplementary Information The online version contains supplementary material available at https://doi.org/10.1007/s43630-025-00684-0.

Acknowledgements The authors thank to Bitlis Eren University Scientific Research Projects Coordination for supporting by the Project BEBAP-2023.25. The authors greatly appreciate Bitlis Eren University for providing experimental research laboratory and softwares (Gaussian 09 and GaussView 5.0). The CQC-IMS is supported by FCT through projects UIDB/00313/2020 (https://doi.org/10.54499/UIDB/00313/2020), UI0313P/QUI/2020 (https://doi.org/10.54499/UIDP/00313/2020). R.F. acknowledges support from Horizon-Widera-2023-Talents-01 ERA-Chair 1011848998 Spectroscopy@IKU *"Manipulating and Characterizing Molecular Architectures: From Isolated Molecules to Molecular Crystals"*.

Author contributions İsa Sıdır: collection of spectroscopic experimental data, initial analysis of the results and interpretation, calculations, writing, editing and funding acquisition. Yadigar Gülseven Sıdır: experiments and funding acquisition. Halil Berber: experiments and funding acquisition. Rui Fausto: data analysis and interpretation, writing, editing and funding acquisition. All authors contribute to the final version of the manuscript.

Declarations

Conflict of interest The authors declare that they have no known competing financial interests or personal relationships that could have appeared to influence the work reported in this paper.

References

1. Hartley, G. S. (1937). The cis-form of azobenzene. *Nature, 140*, 281–281.
2. Rau, H. (2002). *Photoreactive organic thin films* (pp. 3–47). Elsevier.
3. Bandara, H. D., & Burdette, S. C. (2012). Photoisomerization in different classes of azobenzene. *Chemical Society Reviews, 41*, 1809–1825.
4. Rau, H., & Lueddecke, E. (1982). On the rotation-inversion controversy on photoisomerization of azobenzenes. Experimental proof of inversion. *Journal of the American Chemical Society, 104*, 1616–1620.
5. Dürr, H., & Bouas-Laurent, H. (2003). *Photochromism: Molecules and systems*. 1st Edition. Elsevier, Amsterdam.
6. Turanskỳ, R., Konôpka, M., Doltsinis, N. L., Štich, I., & Marx, D. (2010). Switching of functionalized azobenzene suspended between gold tips by mechanochemical, photochemical, and opto-mechanical means. *Physical Chemistry Chemical Physics, 12*, 13922–13932.
7. Henzl, J., Mehlhorn, M., Gawronski, H., Rieder, K., & Morgenstern, K. (2006). Reversible *cis – trans* isomerization of a single azobenzene molecule. *Angewandte Chemie International Edition, 45*, 603–606.
8. Tong, X., Pelletier, M., Lasia, A., & Zhao, Y. (2008). Fast cis–trans isomerization of an azobenzene derivative in liquids and liquid crystals under a low electric field. *Angewandte Chemie International Edition, 47*, 3596–3599.
9. Lenci, F. (2004). *CRC handbook of organic photochemistry and photobiology*. CRC Press.
10. Al-Jebaly, A. M., Hemdan, S. S., & Ali, F. K. (2017). Solvatochromic effect studies on the absorption spectra of 4-[(E)-(3-formayl-4-hydroxyphenyl) diazneyl] benzene sulphonic acid and 2-hydroxy-5-[(E)-(2-nitrophenyl) diazneyl] benzaldehyde azo compounds. *J Sci Hum Stu, 39*, 1–15.
11. Han, M., & Honda, T. (2011). Correlation between the molecular structure and trans ↔ cis isomerization characteristics of azobenzenes. *Science China: Chemistry, 54*, 1955–1961.
12. Ruslim, C., & Ichimura, K. (2000). Spectroscopic and thermal isomerization characteristics of 3, 3′-dialkoxy and dialkanoyloxy azobenzenes. *Journal of Materials Chemistry, 10*, 2704–2707.
13. Bang, C., Shishido, A., & Ikeda, T. (2007). Azobenzene liquid-crystalline polymer for optical switching of grating waveguide couplers with a flat surface. *Macromolecular Rapid Communications, 28*, 1040–1044.
14. Puntoriero, F., Ceroni, P., Balzani, V., Bergamini, G., & Vögtle, F. (2007). Photoswitchable dendritic hosts: A dendrimer with peripheral azobenzene groups. *Journal of the American Chemical Society, 129*, 10714–10719.
15. Parker, R. M., Gates, J. C., Rogers, H. L., Smith, P. G., & Grossel, M. C. (2010). Using the photoinduced reversible refractive-index change of an azobenzene co-polymer to reconfigure an optical Bragg grating. *Journal of Materials Chemistry, 20*, 9118–9125.
16. Ferri, V., Elbing, M., Pace, G., Dickey, M. D., Zharnikov, M., Samorì, P., Mayor, M., & Rampi, M. A. (2008). Light-powered electrical switch based on cargo-lifting azobenzene monolayers. *Angewandte Chemie-International Edition In English-, 47*, 3407.
17. Wen, Y., Yi, W., Meng, L., Feng, M., Jiang, G., Yuan, W., Zhang, Y., Gao, H., Jiang, L., & Song, Y. (2005). Photochemical-controlled switching based on azobenzene monolayer modified silicon (111) surface. *The Journal of Physical Chemistry B, 109*, 14465–14468.
18. Kakiage, K., Yamamura, M., Ido, E., Kyomen, T., Unno, M., & Hanaya, M. (2011). Reactivity of alkoxysilyl compounds: Chemical surface modification of nano-porous alumina membrane using alkoxysilylazobenzenes. *Applied Organom Chemis, 25*, 98–104.
19. Banghart, M. R., Mourot, A., Fortin, D. L., Yao, J. Z., Kramer, R. H., & Trauner, D. (2009). Photochromic blockers of voltage-gated potassium channels. *Angewandte Chemie International Edition, 48*, 9097–9101.
20. Kim, Y., Phillips, J. A., Liu, H., Kang, H., & Tan, W. (2009). Using photons to manipulate enzyme inhibition by an azobenzene-modified nucleic acid probe. *Proceedings of the National academy of Sciences of the United States of America, 106*, 6489–6494.
21. Wang, J., Liu, H.-B., & Ha, C.-S. (2009). Zinc-supported azobenzene derivative-based colorimetric fluorescent 'turn-on'sensing of bovine serum albumin. *Tetrahedron, 65*, 9686–9689.
22. Banghart, M., Borges, K., Isacoff, E., Trauner, D., & Kramer, R. H. (2004). Light-activated ion channels for remote control of neuronal firing. *Nature Neuroscience, 7*, 1381–1386.
23. Norikane, Y., & Tamaoki, N. (2004). Light-driven molecular hinge: A new molecular machine showing a light-intensity-dependent photoresponse that utilizes the trans−cis isomerization of azobenzene. *Organic Letters, 6*, 2595–2598.
24. Murakami, H., Kawabuchi, A., Kotoo, K., Kunitake, M., & Nakashima, N. (1997). A light-driven molecular shuttle based on a rotaxane. *Journal of the American Chemical Society, 119*, 7605–7606.
25. Muraoka, T., Kinbara, K., & Aida, T. (2006). Mechanical twisting of a guest by a photoresponsive host. *Nature, 440*, 512–515.
26. Itoh, M., Harada, K., Kamemaru, S., & Yatagai, T. (2004). Holographic recording on azo-benzene functionalized polymer film. *Japanese Journal of Applied Physics, 43*, 4968.
27. Várhegyi, P., Kerekes, Á., Sajti, S., Ujhelyi, F., Koppa, P., Szarvas, G., & Lörincz, E. (2003). Saturation effect in azobenzene

polymers used for polarization holography. *Applied Physics B: Lasers and Optics, 76*, 397–402.
28. Jiang, X. L., Li, L., Kumar, J., Kim, D. Y., & Tripathy, S. K. (1998). Unusual polarization dependent optical erasure of surface relief gratings on azobenzene polymer films. *Applied Physics Letters, 72*, 2502–2504.
29. Evangelio, E., Saiz-Poseu, J., Maspoch, D., Wurst, K., Busque, F., & Ruiz-Molina, D. (2008). Synthesis, X-ray Structure and reactivity of a sterically protected azobisphenol ligand: on the quest for new multifunctional active ligands. *European Journal of Inorganic Chemistry, 2008*, 2278–2285.
30. Shinkai, S., Nakaji, T., Nishida, Y., Ogawa, T., & Manabe, O. (1980). Photoresponsive crown ethers. 1. Cis-trans isomerism of azobenzene as a tool to enforce conformational changes of crown ethers and polymers. *Journal of the American Chemical Society., 102*, 5860–5865.
31. Luboch, E., Wagner-Wysiecka, E., & Rzymowski, T. (2009). 4-Hexylresorcinol-derived hydroxyazobenzocrown ethers as chromoionophores. *Tetrahedron, 65*, 10671–10678.
32. Luboch, E., Wagner-Wysiecka, E., Poleska-Muchlado, Z., & Kravtsov, V. C. (2005). Synthesis and properties of azobenzocrown ethers with π-electron donor, or π-electron donor and π-electron acceptor group (s) on benzene ring (s). *Tetrahedron, 61*, 10738–10747.
33. Gorostiza, P., & Isacoff, E. Y. (2008). Optical switches for remote and noninvasive control of cell signaling. *Science, 322*, 395–399.
34. Ichimura, K., Oh, S.-K., & Nakagawa, M. (2000). Light-driven motion of liquids on a photoresponsive surface. *Science, 288*, 1624–1626.
35. Stoll, R. S., Peters, M. V., Kuhn, A., Heiles, S., Goddard, R., Bühl, M., Thiele, C. M., & Hecht, S. (2009). Photoswitchable catalysts: Correlating structure and conformational dynamics with reactivity by a combined experimental and computational approach. *Journal of the American Chemical Society, 131*, 357–367.
36. Koshima, H., Ojima, N., & Uchimoto, H. (2009). Mechanical motion of azobenzene crystals upon photoirradiation. *Journal of the American Chemical Society, 131*, 6890–6891.
37. Yamada, M., Kondo, M., Miyasato, R., Naka, Y., Mamiya, J., Kinoshita, M., Shishido, A., Yu, Y., Barrett, C. J., & Ikeda, T. (2008). Photomobile polymer materials—various three-dimensional movements. *Journal of Materials Chemistry, 19*, 60–62.
38. Zhang, Q., & Bazuin, C. G. (2009). Liquid crystallinity and other properties in complexes of cationic azo-containing surfactomesogens with poly(styrenesulfonate). *Macromolecules, 42*, 4775–4786.
39. Khan, A., & Hecht, S. (2006). Towards photocontrol over the helix-coil transition in foldamers: Synthesis and photoresponsive behavior of azobenzene-core amphiphilic oligo(*meta* -phenylene ethynylene)s. *Chemistry A European Journal, 12*, 4764–4774.
40. Khan, A., & Hecht, S. (2006). Poly(*ortho* -phenylene ethynylene) s: Synthetic accessibility and optical properties. *Journal of Polymer Science Part A: Polymer Chemistry, 44*, 1619–1627.
41. Mathews, M., & Tamaoki, N. (2008). Planar chiral azobenzenophanes as chiroptic switches for photon mode reversible reflection color control in induced chiral nematic liquid crystals. *Journal of the American Chemical Society, 130*, 11409–11416.
42. Phillips, J. A., Liu, H., O'Donoghue, M. B., Xiong, X., Wang, R., You, M., Sefah, K., & Tan, W. (2011). Using azobenzene incorporated DNA aptamers to probe molecular binding interactions. *Bioconjugate Chem., 22*, 282–288.
43. Bartels, E., Wassermann, N. H., & Erlanger, B. F. (1971). Photochromic activators of the acetylcholine receptor. *Proceedings of the National academy of Sciences of the United States of America, 68*, 1820–1823.
44. Volgraf, M., Gorostiza, P., Szobota, S., Helix, M. R., Isacoff, E. Y., & Trauner, D. (2007). Reversibly caged glutamate: A photochromic agonist of ionotropic glutamate receptors. *Journal of the American Chemical Society, 129*, 260–261.
45. Wenker, H. (1935). Indicator properties of dinitroaniline azo dyestuffs. *Industrial and Engineering Chemistry Analytical Edition, 7*, 40–41.
46. Escudero, D., Trupp, S., Bussemer, B., Mohr, G. J., & González, L. (2011). Spectroscopic properties of azobenzene-based ph indicator dyes: A quantum chemical and experimental study. *Journal of Chemical Theory and Computation, 7*, 1062–1072.
47. Shi, Y.-W., Liu, X.-Q., Shi, P., & Zhang, X.-Y. (2010). Characterization of zinc-binding properties of a novel imidase from Pseudomonas putida YZ-26. *Archives of Biochemistry and Biophysics, 494*, 1–6.
48. Long, M. E., & Trotter, P. J. (1981). Vibrational manifold considerations for the metal indicator dye 2-(2-pyridylazo)-1-naphthol. *Applied Spectroscopy, 35*, 289–292.
49. He, T., Cheng, Y., Du, Y., & Mo, Y. (2007). Z-scan determination of third-order nonlinear optical nonlinearity of three azobenzenes doped polymer films. *Optics Communications, 275*, 240–244.
50. Sıdır, İ, Sıdır, Y. G., Berber, H., & Fausto, R. (2022). Solvato-, thermo-and photochromism in a new diazo diaromatic dye: 2-(p-tolyldiazenyl) naphthalen-1-amine. *Journal of Molecular Structure, 1267*, 133595.
51. Sıdır, İ, Kara, Y. E., Sıdır, Y. G., Berber, H., & Fausto, R. (2024). Reversal in solvatochromism, photochromism and thermochromism in a new bis-azo dye based on naphthalen-1-amine. *Journal of Photochemistry and Photobiology A: Chemistry, 446*, 115138.
52. Reichardt, C., & Welton, T. (2011). *Solvents and solvent effects in organic chemistry*. John Wiley & Sons.
53. OriginPro. (2021). *(64 bits) (v. 9.8.0.200)*. Northamptom, MA, USA: OriginLab Corporation.
54. Becke, A. D. (1988). Density-functional exchange-energy approximation with correct asymptotic behavior. *Physical Review A, 38*, 3098–3100.
55. Lee, C., Yang, W., & Parr, R. G. (1988). Development of the Colle-Salvetti correlation-energy formula into a functional of the electron density. *Physical Review B, 37*, 785–789.
56. Vosko, S. H., Wilk, L., & Nusair, M. (1980). Accurate spin-dependent electron liquid correlation energies for local spin density calculations: A critical analysis. *Canadian Journal of Physics, 58*, 1200–1211.
57. McLean, A. D., & Chandler, G. S. (1980). Contracted Gaussian basis sets for molecular calculations. I. Second row atoms, Z= 11–18. *The Journal of Chemical Physics, 72*, 5639–5648.
58. Clark, T., Chandrasekhar, J., Spitznagel, G. W., & Schleyer, P. V. R. (1983). Efficient diffuse function-augmented basis sets for anion calculations. III. The 3–21+G basis set for first-row elements, Li–F. *Journal of Computational Chemistry, 4*, 294–301.
59. Frisch, M. J., Pople, J. A., & Binkley, J. S. (1984). Self-consistent molecular orbital methods 25 supplementary functions for Gaussian basis sets. *The Journal of Chemical Physics, 80*, 3265–3269.
60. Gaussian 09, Revision C.01, Frisch, M.J.; Trucks, G.W.; Schlegel, H.B.; et al. Gaussian, Inc, Wallingford CT, 2016.
61. Bauernschmitt, R., & Ahlrichs, R. (1996). Treatment of electronic excitations within the adiabatic approximation of time dependent density functional theory. *Chemical Physics Letters, 256*, 454–464.
62. Casida, M. E., Jamorski, C., Casida, K. C., & Salahub, D. R. (1998). Molecular excitation energies to high-lying bound states from time-dependent density-functional response theory: Characterization and correction of the time-dependent local density approximation ionization threshold. *The Journal of Chemical Physics, 108*, 4439–4449.

63. Frisch, A., Hratchian, H. P., Dennington, R. D., II., Keith, T. A., Millam, J., Nielsen, B., Holder, A. J., & Hiscocks, J. (2009). *GaussView version 50 8*. Wallingford, CT, USA: Gaussian Inc.
64. Chemcraft (Version 1.8), Graphical Software for Visualization of Quantum Chemistry Computations, https://www.chemcraftprog.com/(last access: May 2024).
65. Piyanzina, I., Minisini, B., Tayurskii, D., & Bardeau, J.-F. (2015). Density functional theory calculations on azobenzene derivatives: A comparative study of functional group effect. *Journal of Molecular Modeling, 21*, 34.
66. Brunvoll, J. (1976). The molecular structure of benzene sulphonyl chloride. *Journal of Molecular Structure, 30*, 361–378.
67. Hamm, P., Ohline, S. M., & Zinth, W. (1997). Vibrational cooling after ultrafast photoisomerization of azobenzene measured by femtosecond infrared spectroscopy. *The Journal of Chemical Physics, 106*, 519–529.
68. Lednev, I. K., Ye, T.-Q., Matousek, P., Towrie, M., Foggi, P., Neuwahl, F. V. R., Umapathy, S., Hester, R. E., & Moore, J. N. (1998). Femtosecond time-resolved UV-visible absorption spectroscopy of trans-azobenzene: Dependence on excitation wavelength. *Chemical Physics Letters, 290*, 68–74.
69. Dyck, R. H., & McClure, D. S. (1962). Ultraviolet spectra of stilbene, p-monohalogen stilbenes, and azobenzene and the trans to cis photoisomerization process. *The Journal of Chemical Physics, 36*, 2326–2345.
70. Forber, C. L., Kelusky, E. C., Bunce, N. J., & Zerner, M. C. (1985). Electronic spectra of cis- and trans-azobenzenes: Consequences of ortho substitution. *Journal of the American Chemical Society, 107*, 5884–5890.
71. Cusati, T., Granucci, G., Persico, M., & Spighi, G. (2008). Oscillator strength and polarization of the forbidden n–>pi* band of trans-azobenzene: A computational study. *The Journal of Chemical Physics, 128*, 194312.
72. Kamlet, M. J., Abboud, J. L. M., Abraham, M. H., & Taft, R. W. (1983). Linear solvation energy relationships 23 A comprehensive collection of the solvatochromic parameters, .pi.*, .alpha., and .beta., and some methods for simplifying the generalized solvatochromic equation. *The Journal of Organic Chemistry, 48*, 2877–2887.
73. Kamlet, M. J., Abboud, J. L., & Taft, R. W. (1977). The solvatochromic comparison method 6 The pi* scale of solvent polarities. *Journal of the American Chemical Society., 99*, 6027–6038.
74. Kamlet, M. J., & Taft, R. W. (1976). The solvatochromic comparison method. I. The .beta.-scale of solvent hydrogen-bond acceptor (HBA) basicities. *Journal of the American Chemical Society, 98*, 377–383.
75. Taft, R. W., & Kamlet, M. J. (1976). The solvatochromic comparison method. 2. The .alpha.-scale of solvent hydrogen-bond donor (HBD) acidities. *Journal of the American Chemical Society., 98*, 2886–2894.
76. Catalán, J. (2009). Toward a generalized treatment of the solvent effect based on four empirical scales: dipolarity (SdP, a new scale), polarizability (SP), acidity (SA), and basicity (SB) of the medium. *The Journal of Physical Chemistry B, 113*, 5951–5960.
77. Yanai, T., Tew, D. P., & Handy, N. C. (2004). A new hybrid exchange-correlation functional using the Coulomb-attenuating method (CAM-B3LYP). *Chemical Physics Letters, 393*, 51–57.

Authors and Affiliations

İsa Sıdır[1] · Yadigar Gülseven Sıdır[1] · Halil Berber[2] · Rui Fausto[3,4]

✉ İsa Sıdır
isidir@beu.edu.tr

[1] Department of Physics, Faculty of Sciences and Letters, Bitlis Eren University, 13000 Bitlis, Türkiye

[2] Department of Chemistry, Faculty of Sciences, Eskişehir Technical University, 26470 Eskişehir, Türkiye

[3] CQC–IMS, Department of Chemistry, University of Coimbra, 3004–535 Coimbra, Portugal

[4] Faculty of Sciences and Letters, Department of Physics, Istanbul Kultur University, Ataköy Campus, Bakırköy, 34156 Istanbul, Türkiye